Supporting Information

Banci et al. 10.1073/pnas.1400102111

SI Text

Protein Production. The cDNAs coding for human glutaredoxin 5 (hGRX5) (UniProtKB ID Q86SX6), human iron–sulfur cluster assembly 1 homolog (hISCA1) (UniProtKB ID Q9BUE6), and human iron–sulfur cluster assembly 2 homolog (hISCA2) (UniProtKB ID Q86U28) were acquired from Source BioScience Life Science and, after amplification by PCR, which excludes the mitochondrial targeting sequences (hGRX5, aa 1–34; hISCA1, aa 1–23; and hISCA2, aa 1–43), were inserted into the pETG20A vector, using the Gateway technology (Invitrogen), into the pET15 expression vector (Novagen), using NdeI and BamHI restriction enzymes (Fermentas), and into the pETG-30A vector, using the Gateway technology (Invitrogen), respectively. BL21(DE3)GOLD *Escherichia coli* (Novagen) were transformed with the hGRX5- or hISCA1- or hISCA2-vector, and cells were grown in LB or minimal media [with $(^{15}NH_4)_2SO_4$ and/or [^{13}C]glucose] containing 100 μg/mL ampicillin at 37 °C under vigorous shaking until the OD at 600 nm reached 0.6. For expression of holo hGRX5 and holo hISCA2, cells were grown in the presence of 250 μM $FeCl_3$. Protein expression was induced by adding 1 mM isopropyl β-D-1-thiogalactopyranoside (IPTG) (hGRX5) or 0.2 mM IPTG (hISCA1) or 0.5 mM IPTG (hISCA2) and expression was performed at 25 °C (hGRX5) or 18 °C (hISCA1) or 20 °C (hISCA2) for 14–16 h. Cells were harvested by centrifugation at 6,000 × *g* and resuspended in degassed lysis buffer [50 mM Tris·HCl (pH 8) containing 500 mM NaCl, 5–10 mM imidazole, and 5 mM glutathione (GSH); DTT was used instead of GSH in the case of hISCA1 and hISCA2]. Cells disruption was performed on ice by sonication alternating 30 s of sonication and 5 min of resting for 10 times. All of the following purification steps were performed under anaerobic conditions. The soluble extract, obtained by ultracentrifugation at 40,000 × *g*, was loaded on a HiTrap chelating HP column (GE Healthcare) and the recombinant proteins were eluted with 50 mM Tris·HCl (pH 8), 500 mM NaCl, 5mM GSH/DTT, and 500 mM imidazole. The proteins were then concentrated with an Amicon Ultra-15 centrifugal filter unit with a molecular weight cutoff of 3 kDa (Millipore). Cleavage of the tags was performed by tobacco etch virus protease in 50 mM Tris·HCl (pH 8), 0.5 mM EDTA, 5 mM GSH, and 1 mM DTT overnight at room temperature for hGRX5 and hISCA2 and with thrombin protease (GE Healthcare) in 100 mM Tris, 100 mM NaCl, and DTT 5 mM buffer at pH 8 overnight at 4 °C for hISCA1. These mixtures were loaded again on the His trap column to separate the digested proteins from the tags.

For hGRX5, size-exclusion chromatography was performed as the final purification step using a HiLoad Superdex75 16/60 column (GE Healthcare) and degassed 50 mM phosphate buffer (pH 7), 5 mM GSH, and 5 mM DTT as running buffer, to separate apo hGRX5 from the holo hGRX5. All prepared holo hGRX5 samples contained a residual amount of apo form, ranging from a minimum of 10% to a maximum of 30%. Apo hGRX5 and apo hISCA2 was obtained by treatment of the aerobically purified protein with 100 mM EDTA and 20 mM ferricyanide. After removal of EDTA and ferricyanide by PD-10 desalting column, the proteins were reduced by 10 mM DTT and exchange in the required buffer solution. Whereas the oxidized $[2Fe\text{-}2S]^{2+}$ cluster-bound form of hISCA2 was directly obtained from an anaerobic purification procedure (Fig. S1), the oxidized $[2Fe\text{-}2S]^{2+}$ cluster-bound form of hISCA1 was chemically reconstituted by incubating the purified apo protein in 100 mM Tris, 100 mM NaCl, and 5 mM DTT at pH 8 with two- to fivefold $(NH_4)_2Fe(SO_4)_2$ and Na_2S for 2 h at room temperature. Iron concentration and sulfide content were determined by colorimetric assays as described in Banci et al. (1). An Fe/S/protein ratio of 1:1:1 has been achieved in all preparations, after subtracting the percentage of apo protein in the sample, quantified through ^{1}H-^{15}N heteronuclear single-quantum coherence (HSQC) NMR spectra. Standard MALDI-MS and electrospray ionization-MS experiments were performed for apo hGRX5, apo hISCA1 and apo hISCA2 to confirm the molecular mass of the purified proteins.

Human anamorsin in its [2Fe-2S]–bound state was expressed and purified as previously described (1).

Analytical Gel Filtration, Dynamic Multiangle Light Scattering, and Circular Dichroism. The aggregation state of the apo and holo forms of hGRX5, hISCA1 and hISCA2 was analyzed using analytical gel filtration and/or dynamic multiangle light scattering. Purified samples were loaded on a SuperdexTM 75 HR 10/30 analytical column (Amersham Bioscience). Degassed 50 mM phosphate buffer (pH 7), 5 mM GSH, and 5 mM DTT was used as an eluent. Dynamic multiangle light scattering measurements were performed loading 100 μL of a purified protein sample on a SuperdexTM 75 HR 10/30 analytical column (Amersham Bioscience) connected to the light scattering system Wyatt QELS (Wyatt Technology). Degassed 50 mM phosphate buffer (pH 7) and 5 mM DTT was used as loading and elution buffer at a flow rate of 0.7 mL/min. Whereas hISCA1 switches from a monomer/dimer equilibrium in the apo state to a fully dimeric state in the holo form, hISCA2 is a stable dimer in both apo and holo states.

Far-UV CD spectrum of apo hISCA1 (20 μM) was performed in 10 mM phosphate buffer and 1 mM DTT, pH 7.0. Spectra were acquired at 298 K using a 1-mm path-length cell and a spectropolarimeter (J-810; Jasco). All spectra were recorded with an average of five accumulations at a scan speed of 20 nm/min and at a response time of 2 s. The CD spectrum of apo hISCA1 (Fig. S3) has features characteristic of a folded protein with a large content of β–strands, as indicated by a negative band at 218 nm, and with a lower content of α-helices, as indicated by a negative shoulder at around 225 nm.

UV/Visible and EPR Spectroscopy. UV-visible spectra of holo hGRX5, holo hISCA1, and holo hISCA2 in degassed 50 mM phosphate buffer at pH 7, 5 mM GSH, and 5 mM DTT was performed on a Cary 50 Eclipse spectrophotometer. The absorbance ratio of A_{340}/A_{414} is less than 1.3 as expected in four-cysteine-ligated [2Fe-2S] ferredoxins (2). EPR spectra of hISCA1 with the [2Fe-2S] cluster in the reduced state were recorded in 50 mM phosphate buffer (pH 7) and 10% glycerol with a Bruker Elexsys E500 spectrometer equipped with a X-band microwave bridge (microwave frequency, 9.45 GHz) and an ER 4131 VT (unit for temperature control). EPR parameters were the following: sample temperature 45 K, microwave frequency 9.45 GHz, microwave power 5 mW, modulation frequency 9,387691 GHz, modulation amplitude 2,500 G, and time constant 167 ms. To reduce the cluster, dithionite was added, in a 1:1 protein/dithionite ratio, under anaerobic conditions and the sample was immediately frozen.

Backbone Dynamics of Apo hGRX5 and Apo hISCA1. ^{15}N R_1, R_2, and steady-state heteronuclear NOE experiments were performed at 600 MHz and at 298 K, using the pulse sequences previously reported (3, 4) on ^{15}N-labeled samples. The molecular tumbling values were estimated from the R_2/R_1 ratio using the program QUADRATIC_DIFFUSION (5). The relaxation data for those NHs having an exchange contribution to the R_2 value or exhibiting large-amplitude fast internal motions, as monitored by

low NOE values, were excluded from the analysis (6, 7). Theoretical estimates of the molecular tumbling value under the chosen experimental conditions of magnetic field and temperature were obtained using the program HYDRONMR following the standard procedure (8). The molecular tumbling value of apo hGRX5 (τ_m = 7.97 ± 0.63 ns at 298 K) is in agreement with the theoretical value of the protein in a monomeric state [7.11 ns, calculated through HYDRONMR program (8)]. In agreement with that, analytical gel filtration showed that apo hGRX5 is in the monomeric state (Fig. 4*C*). Except for the N-terminal region and the last two residues at the C terminus that all have negative or very low ^{15}N NOE values, indicating a high degree of flexibility, the ^{15}N backbone relaxation properties show that the protein is essentially a rigid molecule and the loops do not show a high degree of motion (Fig. 4*B*). Indeed, the only additional low ^{15}N{^{1}H} NOE values (<0.5) were found for residues Ser-70 and Thr-108 (Fig. 4*B*); only a few residues (Ser-70, Gln-98, and Thr-108, all located in loop regions, and Cys-122 and Asp-123, located in the first turn of helix α4) show higher R_2 values than the average (Fig. 4*B*), indicating the occurrence of backbone conformational motions in the stretches containing those residues. Moreover, the backbone NH of Gly-68 is not detected, presumably as a consequence of backbone conformational motions acting in the protein region characterized by backbone motions of the close-by NH of Ser-70 and also by the two-residue (Gly-68 and Phe-69) shortening of helix α2 with respect to the holo form.

The ^{1}H-^{15}N HSQC spectrum of apo hISCA1 shows well-dispersed resonances indicative of an essentially folded protein (Fig. S3). However, a number of amide signals are clustered in the spectral region between 8 and 8.5 ppm, typical of unstructured polypeptides. Some residues have more than one signal in the ^{1}H-^{15}N HSQC spectra, thus indicating that the protein has multiple conformations in slow exchange with each other. Furthermore, after 3 d chemical shift dispersion decreases and the number of signals in the ^{1}H-^{15}N HSQC spectral region typical of unstructured proteins increases, demonstrating a general unfolding process of the protein. The presence of multiple conformations and the protein instability prevented a fully backbone resonance assignment. Indeed, only 51 out of 104 expected backbone amide resonances were assigned by standard ^{1}H-detected triple-resonance NMR experiments on 0.5 mM ^{13}C, ^{15}N-labeled samples at 298 K. Analysis of ^{15}N backbone relaxation rates of apo hISCA1 revealed a molecular tumbling value of 9.21 ± 0.83 ns at 298 K, which is higher than expected for a fully monomeric state (7–7.5 ns), supporting the presence of a monomer/dimer equilibrium, which is demonstrated by analytical gel filtration (Fig. S3).

NMR Resonance Assignment of Paramagnetic Signals of Holo hGRX5. The ^{1}H-^{15}N inversion recovery filtered HSQC with antiphase detection (^{1}H-^{15}N IR-HSQC-AP) experiments identified 11 signals that escaped detection using the diamagnetic ^{1}H-^{15}N HSQC. For the above signals, nonselective ^{1}H T_1 relaxation times were measured via a series of inversion recovery HSQC experiments, either using in-phase or the antiphase detection. For the in-phase ^{1}H-^{15}N IR-HSQC, 10 experiments were performed, using inversion recovery delays from 5 ms to 350 ms. Each experiment was obtained by collecting 128 scans each free induction decay (FID), for a 1,024 × 128 data point matrix with a recycle delay of 350 ms. A flip-back pulse was used during the inversion recovery delay to suppress the solvent peak. For the antiphase ^{1}H-^{15}N IR-HSQC spectra, six experiments were performed using inversion recovery delays from 5 to 85 ms. Each experiment was obtained by collecting 900 scans each FID over a 512 × 128 data point matrix with a recycle delay of 93 ms. Water suppression was achieved by a using a soft gradient pulse (0.5%) during the inversion recovery period.

Seven out of 11 signals can be assigned by comparing their observed chemical shifts with the full assignment available for apo hGRX5. Indeed, $[2Fe\text{-}2S]^{2+}$ clusters are expected to provide negligible pseudocontact hyperfine shifts. Therefore, signals belonging to residues in the proximity of the paramagnetic center but not bound to the cluster are expected to experience significant contributions to nuclear relaxation but negligible contributions to their shifts (9), once cluster binding does not induce large structural variations, as in the case of holo hGRX5. The remaining four signals, observed only in the ^{1}H-^{15}N IR-HSQC-AP, are expected to arise from HN groups that, owing to their shorter ^{1}H T_1 values (Table S1), are closer to the paramagnetic center than resonances already assigned. Two of them are those mostly affected by the paramagnetic center both in terms of ^{1}H T_1 relaxation times (9 and 16 ms) and chemical shifts (7.17/131.8 and 7.31/138.1 ppm). Particularly, the ^{15}N chemical shift values of 138 and 131 ppm account for a sizable (about 10–20 ppm) hyperfine contact shift contribution on the ^{15}N spins. This is only consistent with its assignment as the amide group of the iron-bound Cys-67, which therefore displays two signals indicating two backbone conformations of Cys-67 in holo hGRX5. The two last remaining signals, which are very similar to each other in terms of chemical shift (9.31/121.7 and 9.22/121.4 ppm) and ^{1}H T_1 relaxation times (43 and 44 ms), have chemical shifts close to Ser-70 in the apo form (9.98/124.2 ppm) and ^{1}H T_1 values similar to those measured for Lys-59 (50 ms) and Ile-109 (52 ms), whose NHs have a distance from the iron similar to that of Ser-70 in the crystal structure of holo hGRX5. On this basis, we have therefore assigned these two signals to Ser-70, thus identifying two backbone conformations of Ser-70 in holo hGRX5. The only two HN groups that escaped detection in the holo form are those of the two residues following the iron ligand Cys-67 (i.e., Gly-68 and Phe-69). Considering the crystal structure of holo hGRX5, their amide protons are less than 5 Å apart from the metal center (4.8 Å and 4.3 Å, respectively). According to the expected r^{-6} dependence (10), HN signals from Gly-68 and Phe-69 in the holo form should be approximately a factor of two broader than HN signals from Ser-70 or Cys-67 and therefore are beyond the detection limit of the ^{1}H-^{15}N IR-HSQC-AP experiment.

1. Banci L, et al. (2011) Anamorsin is a [2Fe-2S] cluster-containing substrate of the Mia40-dependent mitochondrial protein trapping machinery. *Chem Biol* 18(6):794–804.
2. Wu SP, et al. (2011) Redox chemistry of the Schizosaccharomyces pombe ferredoxin electron-transfer domain and influence of Cys to Ser substitutions. *J Inorg Biochem* 105(6):806–811.
3. Farrow NA, et al. (1994) Backbone dynamics of a free and phosphopeptide-complexed Src homology 2 domain studied by 15N NMR relaxation. *Biochemistry* 33(19): 5984–6003.
4. Grzesiek S, Bax A (1993) The importance of not saturating water in protein NMR. Application to sensitivity enhancement and NOE measurements. *J Am Chem Soc* 115(26):12593–12594.
5. Lee LK, Rance M, Chazin WJ, Palmer AG, 3rd (1997) Rotational diffusion anisotropy of proteins from simultaneous analysis of ^{15}N and ^{13}C alpha nuclear spin relaxation. *J Biomol NMR* 9(3):287–298.
6. Kay LE, Torchia DA, Bax A (1989) Backbone dynamics of proteins as studied by ^{15}N inverse detected heteronuclear NMR spectroscopy: Application to staphylococcal nuclease. *Biochemistry* 28(23):8972–8979.
7. Tjandra N, Feller SE, Pastor RW, Bax A (1995) Rotational diffusion anisotropy of human ubiquitin from 15N NMR relaxation. *J Am Chem Soc* 117(50):12562–12566.
8. García de la Torre J, Huertas ML, Carrasco B (2000) HYDRONMR: Prediction of NMR relaxation of globular proteins from atomic-level structures and hydrodynamic calculations. *J Magn Reson* 147(1):138–146.
9. Banci L, et al. (1994) The three-dimensional structure in solution of the paramagnetic high-potential iron-sulfur protein I from Ectothiorhodospira halophila through nuclear magnetic resonance. *Eur J Biochem* 225(2):715–725.
10. Arnesano F, Banci L, Piccioli M (2005) NMR structures of paramagnetic metalloproteins. *Q Rev Biophys* 38(2):167–219.

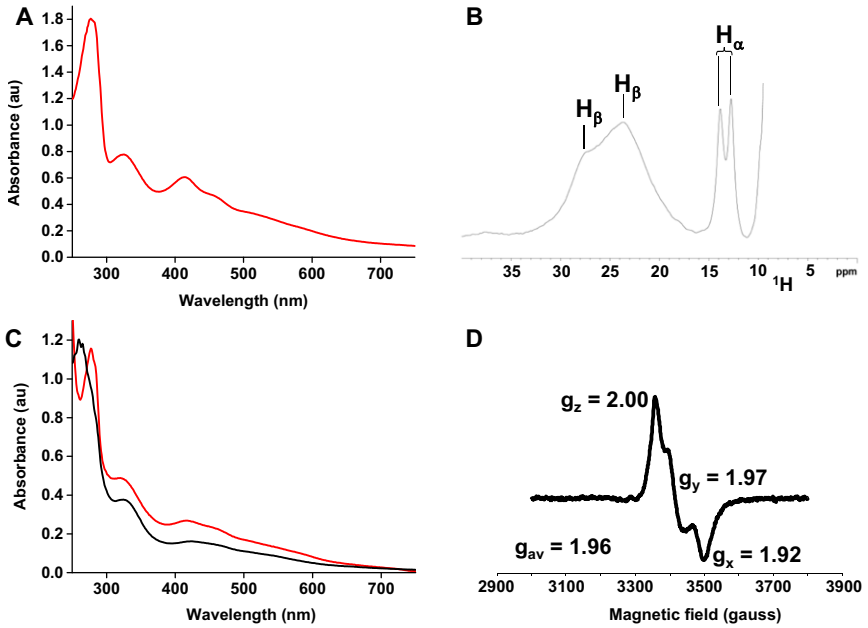

Fig. S1. hGRX5 and hISCA1 bind a [2Fe-2S] cluster. UV/visible (*A*) and paramagnetic 1D ^{1}H NMR (*B*) spectra of holo hGRX5. UV/visible (*C*) and EPR (*D*) spectra of chemically reconstituted holo hISCA1 (in red). The UV/visible spectrum of the holo form of hISCA2, obtained from an anaerobic purification procedure, is reported in black in *C*. EPR spectrum was recorded after the reduction of the sample with one equivalent of dithionite. UV/visible and EPR spectra of holo hISCA1 obtained by mixing holo hGRX5 and apo hISCA1 are the same as those obtained through the chemically reconstitution procedure.

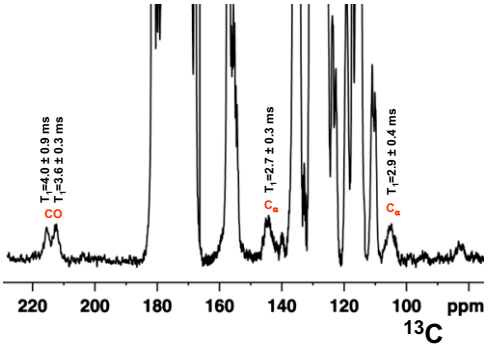

Fig. S2. One-dimensional ^{13}C paramagnetic NMR spectrum of holo hGRX5. The spectrum was recorded, at 298 K, at 175 MHz ^{13}C Larmor frequency. Experimental parameters are described in *Materials and Methods* section. The ^{13}C T_1 values of the identified paramagnetic CO and Cα signals are reported.

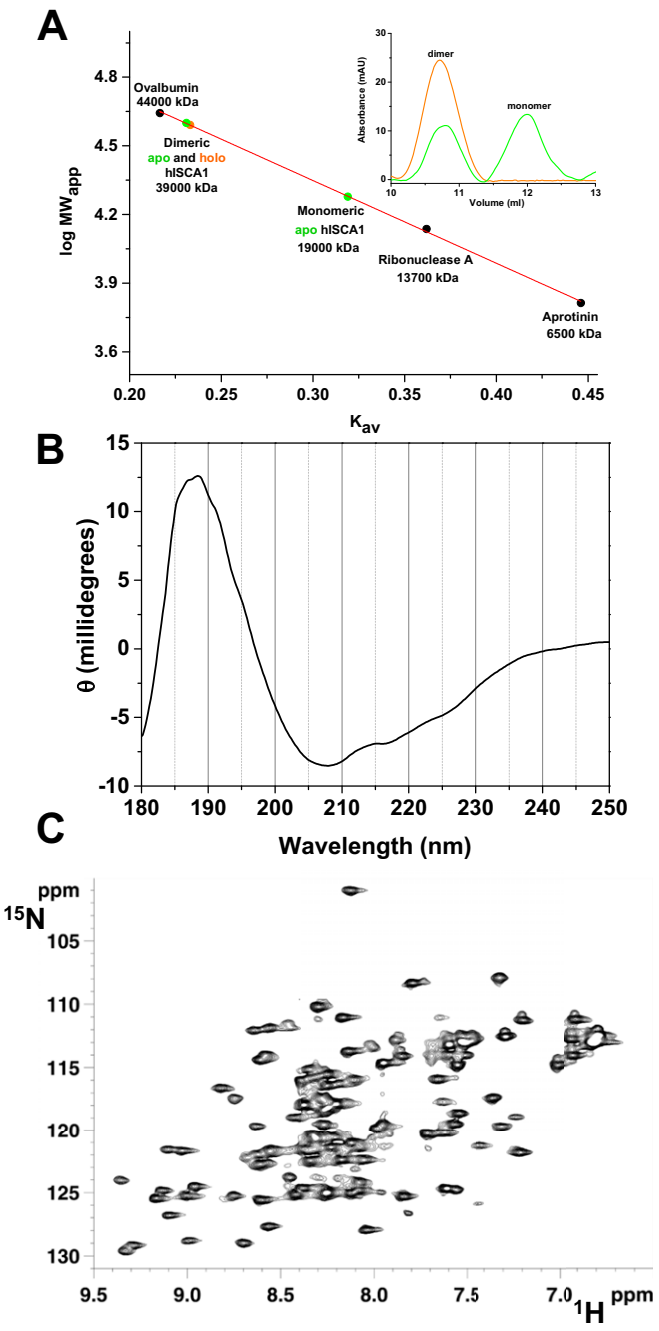

Fig. S3. Aggregation state and structural characterization of apo hISCA1. (*A*) Analytical gel filtration coupled with dynamic multiangle light scattering measurements indicate that apo hISCA1 exists in a monomer/dimer equilibrium, which is shifted to the dimer upon [2Fe-2S] cluster loading. $K_{av} = (V_e - V_0)/(V_t - V_0)$ (V_e, elution volume; V_0, dead volume; V_t, total volume). The monomeric form of apo hISCA1 (in green) runs on gel filtration with an apparent molecular weight (MW_{app}) of 19,000 kDa, which is higher than the expected theoretical value of 12,083 kDa. The dimeric holo hISCA1 (in orange) runs with a MW_{app}, which is twice the MW_{app} of the monomeric apo form. CD (*B*) and ^1H-^{15}N HSQC NMR (*C*) spectra (protein concentration of 20 and 500 μM, respectively) indicate that apo hISCA1 is a folded protein.

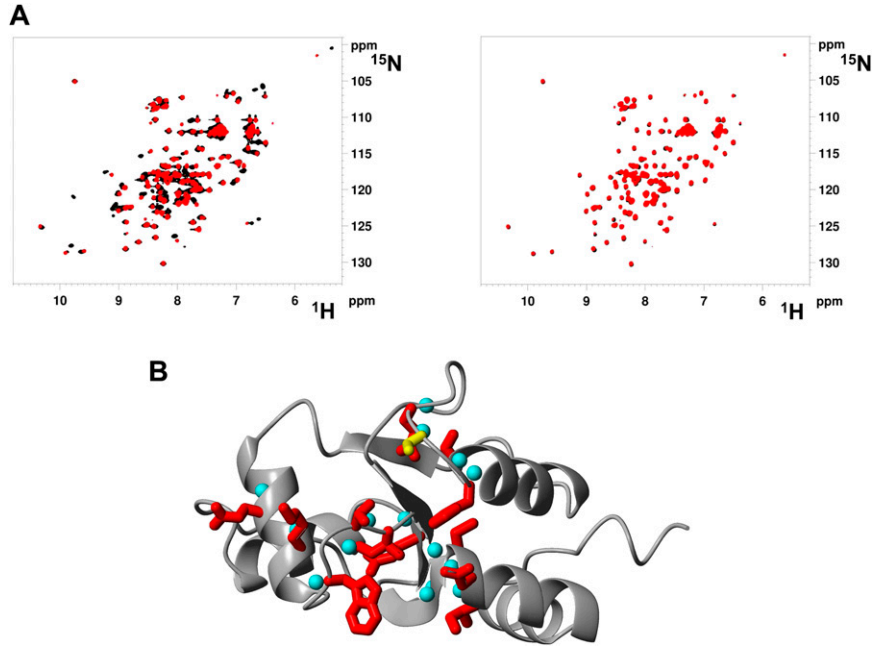

Fig. S4. [2Fe-2S] cluster transfer and protein-protein recognition between hGRX5 and hISCA2. (*A*) Overlays of ^{1}H-^{15}N HSQC spectra of a 1:1 ^{15}N-labeled holo hGRX5/unlabeled apo hISCA2 mixture (red) with ^{15}N-labeled holo hGRX5 (black) (*Left*) and with ^{15}N-labeled apo hGRX5 (black) (*Right*). (*B*) Meaningful Δ_{avg}(HN) chemical shift variations observed between ^{15}N-labeled apo hGRX5 and a 2:1 unlabeled holo hISCA2/^{15}N-labeled apo hGRX5 mixture are mapped on the solution structure of apo hGRX5. Side chains of residues with Δ_{avg}(HN) values greater than the threshold of 0.02 ppm are shown in red and their corresponding backbone HNs are in cyan. Cys-67, also showing a Δ_{avg}(HN) value higher than 0.02 ppm, is in yellow.

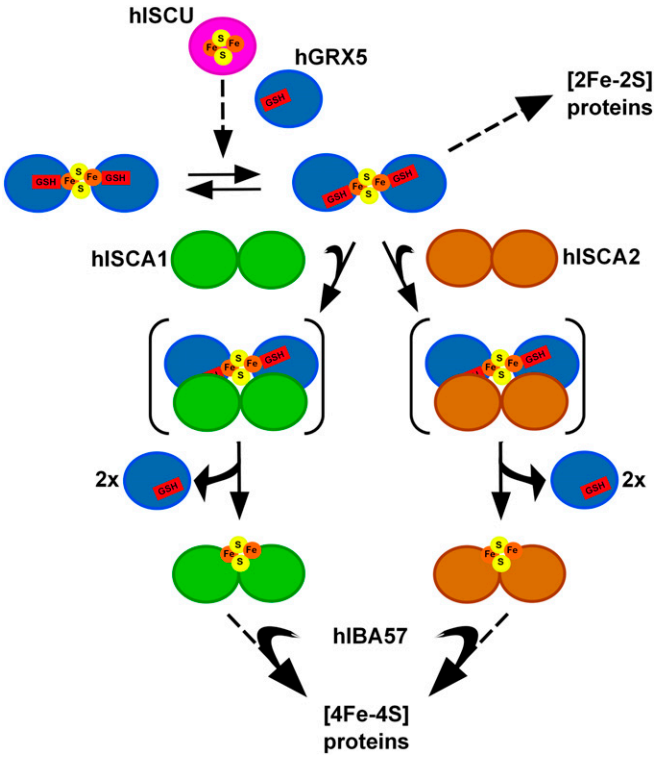

Fig. S5. The [2Fe-2S] transfer process between hGRX5 and hISCA1 and between hGRX5 and hISCA2 in the general context of Fe/S cluster assembly. Apo hGRX5 receives its [2Fe-2S] cluster from the scaffold protein hISCU (1) and transfers it to apo hISCA1, apo hISCA2, and presumably to other mitochondrial [2Fe-2S] partner proteins. Once hISCA1 and hISCA2 have independently received the [2Fe-2S] cluster from hGRX5, they can assemble together and with IBA57 for the maturation of [4Fe-4S] proteins. Undashed arrows represent the pathways investigated in this work. The aggregation state of the protein–protein complexes in parentheses is hypothesized to be heterotetrameric on the basis of the aggregation states of the interacting proteins (i.e., holo hGRX5 with apo hISCA1 or hISCA2).

1. Uzarska MA, Dutkiewicz R, Freibert SA, Lill R, Mühlenhoff U (2013) The mitochondrial Hsp70 chaperone Ssq1 facilitates Fe/S cluster transfer from Isu1 to Grx5 by complex formation. *Mol Biol Cell* 24(12):1830–1841.

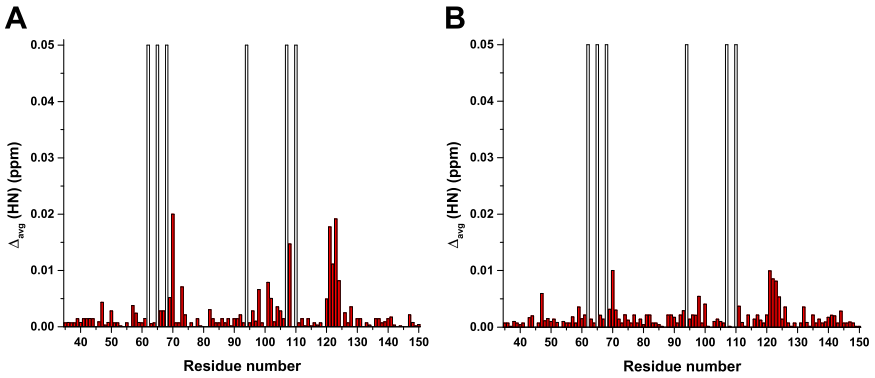

Fig. S6. Apo hGRX5 interacts negligibly with apo hISCA1 and apo hISCA2. Backbone weighted average chemical shift differences Δ_{avg}(HN) between ^{15}N-labeled apo hGRX5 and a 2:1 unlabeled apo hISCA1/^{15}N-labeled apo hGRX5 mixture (*A*) or a 2:1 unlabeled apo hISCA2/^{15}*N*-labeled apo hGRX5 mixture (*B*). White bars indicate Pro residues and the unassigned backbone NH of Gly-68.

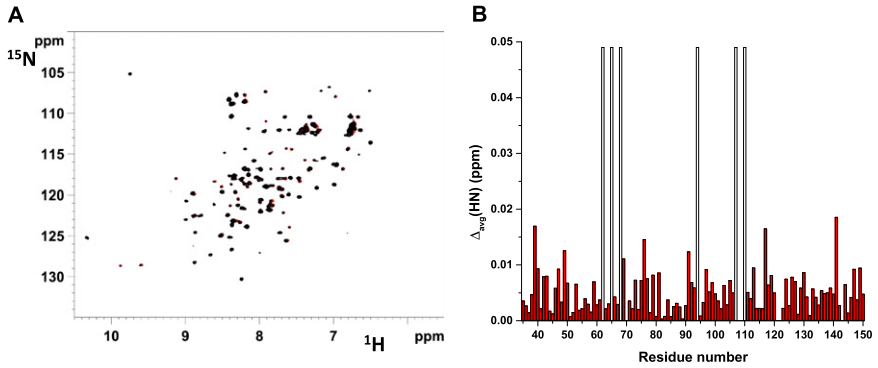

Fig. S7. Holo hGRX5 does not interact with apo anamorsin. (*A*) Overlay of ^{1}H-^{15}N HSQC spectra of ^{15}N-labeled apo hGRX5 (red) and a 2:1 unlabeled [2Fe-2S]-anamorsin/^{15}N-labeled apo hGRX5 mixture (black). (*B*) Backbone weighted average chemical shift differences Δ_{avg}(HN) between ^{15}N-labeled apo hGRX5 and a 2:1 unlabeled [2Fe-2S]-anamorsin/^{15}N-labeled apo hGRX5 mixture. White bars indicate Pro residues and the unassigned backbone NH of Gly-68.

Table S1. Chemical shifts and ^{1}H T_1 values of residues close (within 10 Å) to the paramagnetic $[2Fe\text{-}2S]^{2+}$ center in holo hGRX5

Residue	^{1}H/^{15}N chemical shifts, ppm	T_1, ms
Lys-59	8.38/117.6	50 ± 10
Gly-60	7.90/115.0	84 ± 5
Gln-66	8.72/120.1	55 ± 5
Cys-67$_a$	7.17/131.8	9 ± 5
Cys-67$_b$	7.31/138.1	16 ± 4
Gly-68	—	—
Phe-69	—	—
Ser-70$_a$	9.31/121.7	43 ± 3
Ser-70$_b$	9.22/121.4	44 ± 4
Asn-71	8.64/118.8	125 ± 25
Ala-72	8.08/121.6	—
Leu-91	8.05/118.8	165 ± 35
Ile-109	8.43/120.2	52 ± 5

Table S2. Statistical analysis of the final REM family of apo hGRX5

Statistics	REM* (20 structures)
Rmsd per distance constraint,[†] Å	
Intraresidue (555)	0.0245 ± 0.0012
Sequential (549)	0.0220 ± 0.0011
Medium-range (439)[‡]	0.0189 ± 0.0011
Long-range (456)	0.0212 ± 0.0019
Total (1999)	0.0220 ± 0.0008
Rmsd per dihedral angle constraints,[†] °	
Phi (94)	0.84 ± 0.28
Psi (92)	1.57 ± 0.23
Average no. of NOE violations larger than 0.3 Å	0.00 ± 0.00
Average NOE deviation,[§] Å^2	1.08 ± 0.068
Average angle deviation,[§] rad^2	0.10 ± 0.022
Rmsd to the mean structure,[¶] Å (BB)	0.45 ± 0.08
(HA) [¶]	0.80 ± 0.08
Structural analysis[‖]**	
% of residues in most favorable regions	91.2%
% of residues in allowed regions	8.1%
% of residues in generously allowed regions	0.7%
% of residues in disallowed regions	0%
G-factor	−0.41
Structure Z-scores**,[††]	
First-generation packing quality	0.7
Second-generation packing quality	4.9
Ramachandran plot appearance	−2.4
$\chi1/\chi2$ rotamer normality	−4.0
Backbone conformation	−0.1
RMS Z-score**,[††]	
Bond lengths	1.2
Bond angles	0.8
Omega angle restraints	1.9
Side chain planarity	1.4
Improper dihedral distribution	1.3
Inside/outside distribution	1.0

*REM indicates the restrained energy minimized family of 20 structures.

[†]The number of meaningful constraints for each class is reported in parentheses.

[‡]Medium-range distance constraints are those between residues (i,i+2), (i,i+3), (i,i+4), and (i,i+5).

[§]NOE and torsion angle constraints were applied with force constants of 50 kcal·mol^{-1}·Å^{-2} and 32 kcal·mol^{-1}·rad^{-2}, respectively.

[¶]The rmsd to the mean structure is reported considering the segments 42–66, 70–107, and 109–149.

[‖]As it results from the Ramachandran plot analysis. For the PROCHECK statistics, an overall G-factor larger than −0.5 is expected for a good-quality structure.

[**]The statistic analysis is reported considering the segments 42–66, 70–107, and 109–149.

[††]Values based on WHAT-IF output. A Z-score is defined as the deviation from the average value for this indicator observed in a database of high-resolution crystal structures, expressed in units of the SD of this database-derived average. Typically, Z-scores below a value of −3 are considered poor, and those below −4 are considered bad.